JOURNAL OF GENERAL VIROLOGY

RESEARCH ARTICLE

Stevenson-Leggett *et al.*, *Journal of General Virology* 2021;102:001642

DOI 10.1099/jgv.0.001642

MICROBIOLOGY SOCIETY

OPEN ACCESS

Analysis of the avian coronavirus spike protein reveals heterogeneity in the glycans present

Phoebe Stevenson-Leggett[1], Stuart Armstrong[2], Sarah Keep[1], Paul Britton[1] and Erica Bickerton[1,*]

Abstract

Infectious bronchitis virus (IBV) is an economically important coronavirus, causing damaging losses to the poultry industry worldwide as the causative agent of infectious bronchitis. The coronavirus spike (S) glycoprotein is a large type I membrane protein protruding from the surface of the virion, which facilitates attachment and entry into host cells. The IBV S protein is cleaved into two subunits, S1 and S2, the latter of which has been identified as a determinant of cellular tropism. Recent studies expressing coronavirus S proteins in mammalian and insect cells have identified a high level of glycosylation on the protein's surface. Here we used IBV propagated in embryonated hens' eggs to explore the glycan profile of viruses derived from infection in cells of the natural host, chickens. We identified multiple glycan types on the surface of the protein and found a strain-specific dependence on complex glycans for recognition of the S2 subunit by a monoclonal antibody *in vitro*, with no effect on viral replication following the chemical inhibition of complex glycosylation. Virus neutralization by monoclonal or polyclonal antibodies was not affected. Following analysis of predicted glycosylation sites for the S protein of four IBV strains, we confirmed glycosylation at 18 sites by mass spectrometry for the pathogenic laboratory strain M41-CK. Further characterization revealed heterogeneity among the glycans present at six of these sites, indicating a difference in the glycan profile of individual S proteins on the IBV virion. These results demonstrate a non-specific role for complex glycans in IBV replication, with an indication of an involvement in antibody recognition but not neutralisation.

INTRODUCTION

Infectious bronchitis is a highly contagious disease of chickens that manifests primarily through respiratory clinical signs in infected birds, caused by the *Gammacoronavirus* infectious bronchitis virus (IBV). Some strains of IBV also cause renal and reproductive disease, with infection resulting in major economic losses to the poultry industry worldwide due to reductions in egg production and meat quality [1–4]. IBV has a positive-sense single-stranded RNA genome of 27.6 kb, encoding four structural proteins including a large glycoprotein on the surface of the virion known as the spike (S) protein. The S protein is displayed as trimers protruding from the viral membrane [5]. Each S protein comprises two subunits known as S1 and S2, responsible for attachment and fusion of viral and cellular membranes during IBV infection, respectively. It has been demonstrated in several studies that the S protein is a determinant of *in vitro* tropism for IBV [6–9]. Recent research has described the complex structure of coronavirus S proteins by using cryo-electron microscopy (EM) techniques [5, 10, 11]. These, and subsequent studies, have revealed the multi-domain structure of the S protein and alluded to the importance of protein folding and epitope presentation in the function of the protein [12, 13].

Received 09 April 2021; Accepted 04 July 2021; Published 23 August 2021

Author affiliations: [1]The Pirbright Institute, Woking, Surrey GU24 0NF, UK; [2]Institute of Infection and Global Health, University of Liverpool, Liverpool L3 5RF, UK.

***Correspondence:** Erica Bickerton, erica.bickerton@pirbright.ac.uk

Keywords: antibody; coronavirus; glycosylation; neutralisation; spike protein; type I membrane protein.

Abbreviations: BES, N,N-bis(2-hydroxyethyl)-2-aminoethanesulfonic acid; CH, central helix; CK, chicken kidney; CTD, C-terminal domain; DMEM, Dulbecco's modified essential medium; DTT, dithiothreitol; EM, electron microscopy; ER, endoplasmic reticulum; FBS, foetal bovine serum; FP, fusion peptide; GDE, glycan-dependent epitope; HA, haemagglutinin; HIV, human immunodeficiency virus; hpi, hours post-infection; HR2, heptad repeat 2; HVR-1, hypervariable region 1; IBV, infectious bronchitis virus; IF, immunofluorescence; Kif, kifunensine; LC, liquid chromatography; mAb, monoclonal antibody; MOI, multiplicity of infection; MS, mass spectrometry; N, asparagine; NTD, N-terminal domain; PBS, phosphate buffered saline; PRNT, plaque reduction neutralisation titre; RBD, receptor binding domain; rIBV, recombinant IBV; RIR, Rhode Island Red; S, spike; SARS-CoV, severe acute respiratory syndrome coronavirus; SDS-PAGE, sodium dodecyl sulphate-polyacrylamide gel electrophoresis; SPF, specific pathogen free; UT, untreated.

One supplementary figure is available with the online version of this article.

The post-translational modification of proteins by N-glycosylation is an essential process in protein synthesis and is critical for folding in the endoplasmic reticulum (ER) and Golgi [14, 15]. Similarly to other RNA virus attachment proteins, including influenza haemagglutinin (HA) and HIV-1 gp120 [16, 17], the S protein of IBV displays a high-level N-linked glycosylation on its surface [5, 18, 19]. N-glycosylation occurs at asparagine (N) residues in the amino acid motif asparagine-x-serine/threonine (N-X-S/T) [15, 20]. N-glycosylation in the spike protein of human coronaviruses has been investigated, with a recent boom in studies assessing the spike protein of newly emerged severe acute respiratory syndrome coronavirus 2 (SARS-CoV-2) [13, 21–23]. Previous analysis of IBV strains using bioinformatic techniques identified 30 such sites present in the sequences of strains belonging to the Massachusetts serotype, with the total number of predicted sites varying between serotypes and strains [24]. The pathway of N-linked glycosylation begins in the ER and progresses through the Golgi network, where different monosaccharide molecules are sequentially removed from and added to oligosaccharide branches, until the protein has reached its final conformation. Different types of glycan emerge from this process, attached to a given protein, and are produced as a result of the actions of a variety of cellular enzymes including the ER mannosidase α-mannosidase I, which is responsible for the cleavage of alpha 1,2 mannose linkages, from Man9GlcNAc2 to Man8GlcNAc2 and is one of a range of mannose-trimming enzymes [25]. Three types of glycan have been described – simple or oligomannose-type, which consist of mainly mannose molecules, complex glycans comprising multiple monosaccharide types, and hybrid glycans, which are made up of both mannose and complex oligosaccharides [26]. N-linked glycosylation is a cellular process of post-translational modification and as such this process varies by cell type and host species, thus the selection of propagation method for studying viral protein glycosylation is an important consideration, especially for animal viruses [27, 28].

The role of N-linked glycosylation in viral proteins is an ever-growing field of investigation, informing many aspects of virus research and vaccine design, as recently reviewed by Watanabe and colleagues [29]. For human immunodeficiency virus (HIV-1), glycosylation in the viral glycoprotein gp120 is strongly linked to antibody neutralization, with the protein exhibiting glycan-dependent epitopes (GDEs) on its surface [30–32]. In influenza viruses, mutations in glycosylation sites can alter virulence and immune response to the virus [33, 34]. Evolution of the glycan shield in influenza has also been observed, with the recent characterization of HIV-1 positive serum capable of neutralizing both HIV and influenza H3N2 viruses, due to recognition and specificity to similar glycan structures on the attachment proteins in each virus [35]. Previous studies have also characterized glycosylation in the coronavirus S protein, highlighting its relevance to different stages of the virus lifecycle as well as its antigenicity and roles in epitope masking [10, 13]. Studies with the *Betacoronavirus* SARS-CoV have noted the importance of glycans in cellular entry mechanisms [36]. More recently, a detailed picture of glycosylation in the SARS-CoV-2 S glycoprotein was elucidated, offering a basis for the investigation of novel vaccine targets [22]. The glycosylation profile of the IBV S protein has been described in most detail for a Vero cell-adapted strain of Beaudette and in recombinant M41 proteins expressed from insect cells [5, 18]. Recent research shows that glycosylation in the M41 S protein is necessary for binding to host cells as well as determining receptor specificity [19, 37]. These investigations present valuable contributions to understanding the role of S protein glycosylation, with the caveat of protein expression in insect or mammalian cells, and in some cases analysis of glycosylation in the M41 receptor binding domain (RBD) only [19]. Expression of shorter sections of glycoproteins in this context has been shown to impact the glycan composition in HIV, where the amounts of oligomannose-type glycans were decreased in the monomeric form of the protein compared to the trimer [38]. Cell type has also been shown to influence the glycan make up of a glycoprotein, with mammalian and avian cells, for example, affecting the proportions of glycan types present on the resulting glycoproteins [27]. Studies with influenza have alluded to the impacts of these differences on vaccine design, highlighting the importance of the selection of appropriate propagation methods [39].

To explore the glycosylation of the IBV S protein produced by a method more representative of the natural host, we have analysed the glycan profile of the IBV S proteins from two different strains of IBV, the pathogenic M41-CK strain [40] and the attenuated recombinant IBV (rIBV) Beau-R, a molecular clone of the attenuated Beau-CK strain [41]. Both M41-CK and Beau-R were propagated in embryonated specific pathogen-free (SPF) chicken eggs and the glycan profiles and the role of glycosylation were assessed in chicken cells including primary chicken (CK) cells and DF-1 cells, with a focus on the role of complex glycans in antibody recognition, viral replication and infectivity. Egg-derived IBV is used for infection studies and production of highly successful live attenuated vaccines, demonstrating that IBV obtained in this manner is still infectious and can either result in infection of chickens or for protection against infection and disease. Using the α-mannosidase I inhibitor, kifunensine, to inhibit complex glycan formation, we have identified a strain-specific change in spike protein recognition by a monoclonal antibody (mAb). The glycan profile of the S protein of M41-CK, propagated in chicken eggs, was further investigated using mass spectrometry, showing that the majority of predicted glycosylation sites on the surface of the protein are indeed glycosylated, and that there is a degree of heterogeneity in the glycan structures present at each site.

METHODS

Cells and viruses

All IBV stocks were propagated in 10-day-old specific pathogen-free (SPF) Rhode Island Red (RIR) embryonated hens' eggs. M41-CK (GenBank accession number MK728875.1) is a pathogenic IBV belonging to the GI-1

genotype and Massachusetts serotype that has been adapted for propagation in primary chicken kidney (CK) cells [40, 42, 43] through serial passage in CK cells. Beau-R [41] is a molecular clone of Beau-CK, the CK cell-adapted Beaudette strain (GenBank accession number AJ311317) also belonging to the GI-1 genotype and Massachusetts serotype. Unlike M41-CK, Beau-R exhibits an extended host tropism, allowing propagation in DF-1 cells [6, 44].

CK cells were prepared using kidneys from 2- to 3-week-old SPF RIR chickens by the central services unit at The Pirbright Institute [45]. DF-1 cells were obtained from Central Services Unit at The Pirbright Institute and maintained in Dulbecco's modified essential medium (DMEM, Sigma-Aldrich, St Louis, MO, USA) with 10% foetal bovine serum (FBS, Sigma-Aldrich, St Louis, MO, USA). All cells were maintained at 37 °C in 5% CO_2.

Enzymatic deglycosylation of purified IBV

M41-CK and Beau-R were purified by ultracentrifugation of allantoic fluid through a 30–60% sucrose gradient. Samples of 10 µl of each virus were subjected to digestion with either EndoH or PNGase F (both New England Biolabs, Ipswich, MA, USA) for 1 h at 37 °C, according to the manufacturer's instructions. Following digestion, enzymes were heat-inactivated at 65 °C for 20 min. Samples were analysed by SDS-PAGE followed by Western blot using the monoclonal antibody anti-S2 26.1 (PrioMab, ThermoFisher, Waltham, MA, USA).

IBV infections in the presence of kifunensine

CK cells seeded in six-well tissue-culture plates were washed once in PBS and infected with either M41-CK or Beau-R diluted in serum-free medium (1XBES) [46] at an approximate m.o.i. of 0.01. For treated samples, kifunensine (Sigma-Aldrich, St Louis, MO, USA) was added to the diluted virus at the time of infection at a final concentration of 20 µm. Infected cells were incubated in virus inoculum for 1 h at 37 °C (5% CO_2) before washing once in PBS and the addition of 1 X N,N-bis(2-hydroxyethyl)−2-aminoethanesulfonic acid (BES) [46] medium to each well (1 ml for 24-well plates, 3 ml for six well plates). Supernatant was harvested after 24 h incubation at 37 °C (5% CO_2).

For assessment of replication kinetics, cells were infected as described above. After 1 h incubation cells were washed twice in PBS and 3 ml of fresh 1XBES medium was added to each well, either neat or containing kifunensine at a final concentration of 20 µm. Supernatant was harvested at 1, 24, 48, 72 and 96 h post-infection. Viral titres in each sample were assessed by plaque assay in CK cells. To quantify the intracellular titre, cells were washed once in PBS and fresh medium was added to each well (following supernatant harvesting) into which the cells in each well were scraped. Cells were then subjected to freeze-thaw (−80/37 °C) to lyse the cells before titration by plaque assay in CK cells.

Analysis of protein expression by estern blot

Infected cells were washed once in cold PBS and incubated in 350 µl RIPA lysis buffer (ThermoFisher, Waltham, MA, USA) for 20 min on ice. Cells were scraped into the buffer using a cell scraper and centrifuged at 9000 ***g*** for 3 min in a refrigerated centrifuge. Cell pellets were discarded, and cell lysates were thawed at room temperature and diluted 3:1 with Laemmli Sample Buffer (SB, 4X, Bio-Rad, Santa Rosa, CA, USA) containing β-mercaptoethanol (Sigma-Aldrich, MO, USA). Diluted samples were heated to 80 °C for 10 min before loading on to a Bio-Rad Protean Mini-TGX sodium dodecyl sulphate-polyacrylamide gel electrophoresis (SDS-PAGE) gel (4–20%). Samples were run for 1 h at 150 V alongside Bio-Rad Protein Dual Colour Standard. Proteins were transferred onto a nitrocellulose membrane following the Bio-Rad Trans-Blot turbo transfer protocol for Mini-TGX gels. Membranes were blocked for 1 h in PBS containing 0.1% Tween 20 and 5% Marvel milk powder. Primary antibodies were diluted in the same blocking solution and applied to membranes for 1 h at room temperature. Membranes were blocked in 5% Marvel milk powder in PBS containing 0.1% Tween 20 (Sigma-Aldrich, St Louis, MO, USA) for 1 h at room temperature. Antibody solutions were prepared in blocking solution. Anti-S2 (26.1, PrioMab, Waltham, MA, USA) was diluted 1:500, anti-E (produced in house) was diluted 1:1000 and anti-β-actin (Abcam, Cambridge, UK) was diluted 1:1000. Membranes were incubated in primary antibody solutions for 1 h at room temperature before 3×5 min washes in PBS-Tween. Secondary antibodies (LI-COR Biosciences, Lincoln, NE, USA) were diluted 1:15000 in blocking solution. Membranes were subjected to three further washes in PBS-Tween followed by a single wash in distilled water. Membranes were visualized following the estern blot protocol on a LI-COR Odyssey Scanner using both 700 and 800CW channels.

Plaque reduction assays

Samples of M41-CK and Beau-R infected CK cell supernatant from untreated and kifunensine treated cells were diluted to 2000 p.f.u. in BES medium and used to serially dilute either A13 [47] or M41-CK polyclonal sera (collected 14 days post-challenge from 43-day-old SPF Rhode Island Red chickens challenged with M41-CK [48]) twofold, up to 1:1024. These mixtures were incubated with constant agitation for 30 min at room temperature. The quantity of non-neutralized virus in each dilution mixture was then determined by plaque assay in CK cells. Plaque reduction neutralization ($PRNT_{50}$) values were calculated using the Reed-Muench method [49].

Immunofluorescence (IF) with confocal microscopy analysis

Cells seeded onto glass coverslips in 24-well tissue culture plates to approximately 80% confluency were washed once in PBS and infected with IBV at an m.o.i. of 1 (diluted in BES medium). Cells were incubated at 37 °C (5% CO2) for 1 h then virus inoculum was removed and replaced with serum-free medium. Cells were incubated for a further 23 h

at 37 °C before fixation in 4% paraformaldehyde in PBS for 20 min at room temperature. Following fixation, cells were permeabilized with 0.1% Triton X-100 in PBS for 10 min at room temperature. Cells were washed once in PBS then incubated for 1 h in a blocking solution of PBS containing 0.5% bovine serum albumin (BSA, Sigma, St Louis, MO, USA) in PBS. Cells were incubated in primary antibody for 1 h at room temperature then subjected to 3×5 min washes in PBS before incubation in secondary antibody solutions for 1 h at room temperature. Primary antibodies included anti-S2 (26.1, 1:500) and anti-tubulin (1:1000, Abcam, Cambridge, UK). Secondary antibodies, AlexaFluor goat anti-mouse 488 and 568 (Invitrogen, Carlsbad, CA, USA), were diluted 1:500 in blocking solution. Cells were washed a further three times in PBS before nuclei were counterstained with DAPI, diluted 1:15000 in water, for 5 min at room temperature. Cells were washed once more in water before the coverslips were mounted onto glass microscope slides using VectaShield (Vector Labs, Burlingame, CA, USA). Coverslips were sealed with nail varnish and stored at 4 °C before examination under a Leica confocal microscope.

Mass spectrometry: N-glycosylation mapping

Protein digestion

Purified IBV M41-CK was diluted with 50 mm ammonium bicarbonate (NH_4HCO_3, Sigma-Aldrich). Proteins were reduced addition of dithiothreitol (DTT, Sigma, 3 mm final) and heated at 60 °C for 10 min. The samples were returned to room temperature, and iodoacetamide (Sigma, 9 mm final) added for 30 min in the dark to alkylate the proteins. The sample was split, and proteins were digested with either trypsin or chymotrypsin (Sigma) and left to incubate at 37 °C overnight. The resulting peptide samples were then dried using a centrifugal vacuum concentrator (Eppendorf). Deglycosylation and $H_2{}^{18}O$ labelling was performed as described by Zhang *et al.* [50]. Peptides were resuspended in 50 mm ammonium bicarbonate buffer prepared in $H_2{}^{18}O$ (97% ^{18}O, Sigma Aldrich). The peptide samples were split and PNGase F (Sigma) added to only one of the samples and incubated at 37 °C for 2 h. Samples were then acidified with trifluoroacetic acid [1% (v/v) final]. Peptides were concentrated and desalted using C18 Stage tips (ThermoFisher Scientific) and then samples dried using a centrifugal vacuum concentrator (Eppendorf). Peptides were resuspended in 0.1% (v/v) trifluoroacetic acid and 5% (v/v) acetonitrile.

NanoLC MS ESI MS/MS analysis

Peptides were analysed by on-line nanoflow LC using the Ultimate 3000 nano system (Dionex/Thermo Fisher Scientific). Samples were loaded onto a trap column (ThermoScientific, PepMap100, C18, 300 µm×5 mm) then resolved on an analytical column (Easy-Spray PepMap RSLC 50 cm×75 µm inner diameter, C18, 2 µm, 100 Å) fused to a silica nanoelectrospray emitter (Dionex). The column was operated at a constant temperature of 30 °C and the LC system coupled to a Q-Exactive HF mass spectrometer (Thermo Fisher Scientific). Chromatography was performed with a buffer system consisting of 0.1% formic acid (buffer A) and 80% acetonitrile in 0.1% formic acid (buffer B). The peptides were separated by a linear gradient of 3.8–50% buffer B over 90 min at a flow rate of 300 nl min^{-1}. The Q-Exactive HF was operated in data-dependent mode with survey scans acquired at a resolution of 60000 and scan range 350–2000 m/z. Up to the top 10 most abundant isotope patterns with charge states+2 to+5 from the survey scan were selected with an isolation window of 2.0 Th and fragmented by higher-energy collisional dissociation with normalized collision energies of 30. The maximum ion injection times for the survey scan and the MS/MS scans were 100 and 45 ms, respectively, and the ion target value was set to 3E6 for survey scans and 1E5 for the MS/MS scans. MS/MS events were acquired at a resolution of 30000. Repetitive sequencing of peptides was minimized through dynamic exclusion of the sequenced peptides for 20 s.

Bioinformatic analysis

Spectral data were analysed using the PEAKS studio 8.5 software (Bioinformatics Solutions, Waterloo, ON, Canada). Tandem MS data were searched against the predicted protein sets of IBV strain M41 (Uniprot, June 2015) and *Gallus gallus* (NCBI RefSeq Feb. 2016) (46255 sequences combined). Search parameters were as follows; precursor mass tolerance set to 10 ppm and fragment mass tolerance set to 0.05 Da. Two missed tryptic cleavages were permitted. Carbamidomethylation (cysteine) was set as a fixed modification and oxidation (methionine), HexNAcetylation (asparagine,+203.08 Da), deamidation of asparagine (+0.9840 Da), and deglycosylated asparagine ^{18}O labelling (+2.9890 Da) were set as variable modifications. The search was semi-specific and the PEAKs PTM profiling function was utilized. An Ascore of 20 was required for a confident PTM determination. The PTM false discovery rate was set at 1%.

Mass spectrometry (MS): Glycan analysis

Protein digestion

Purified IBV was diluted with 50 mm ammonium bicarbonate (Sigma-Aldrich) and 0.1% (w/v) Rapigest (Waters, Elstree, UK). Samples were then incubated at 80 °C for 10 min and reduced with 3 mm DTT at 60 °C for 10 min then alkylated with 9 mm iodoacetamide at room temperature for 30 min in the dark. The sample was split, and proteins were digested with either trypsin or chymotrypsin (Sigma) and left to incubate at 37 °C overnight. Samples were then acidified with trifluoroacetic acid (1% (v/v) final) and precipitated Rapigest removed. Peptides were concentrated and desalted using C18 Stage tips (ThermoFisher Scientific) and then samples dried using a centrifugal vacuum concentrator (Eppendorf). Peptides were resuspended in 0.1% (v/v) trifluoroacetic acid and 5% (v/v) acetonitrile.

LC MS/MS

LC-MS/MS analysis was performed on an Orbitrap Fusion Tribrid mass spectrometer (ThermoScientific), attached to an Ultimate 3000 nano system (Dionex). Peptides were loaded onto the trapping column (ThermoScientific, PepMap100,

C18, 300 µm×5 mm), and then resolved on an analytical column (Easy-Spray C18 75 µm×500 mm 2 µm bead diameter column) using a 30 min gradient from 96.2% A (0.1% FA) and 3.8% B (80% MeCN 19.9% H_2O 0.1% FA) to 50% B at a flow rate of 300 nl min−1. The mass spectrometer was operated in data-dependent mode to automatically switch between MS and MS/MS acquisition using HCD and EThcD. MS1 scan was acquired from 450 to 1800 m/z (60000 resolution, 4e5 AGC, 50 ms injection time) followed by EThcD MS/MS acquisition of the precursors with the highest charge states in an order of intensity and detection in the Orbitrap. HCD (30000 resolution, 3e5 AGC, 60 ms injection time, collision energy (%)=28). ETD scan range 120–2000 m/z (30000 resolution, 1e5 AGC, 120 ms injection time). The Fusion was run in product-dependent acquisition mode (HCDpdETD), which generates a pair of HCD and ETD spectra. Acquisition was triggered when fingerprint ions [m/z 204.0867(HexNac), 138.0545(HexNac fragment), and 366.1396(HexNacHex)] were detected within top 20 product ions.

Data analysis

HCDpdETD data was searched against IBV strain M41 (UniProt, June 2015) proteins using Byonic (v4.0.12, Protein Metrics). The search parameters were as follows: Trypsin (RK) and Chymotrypsin (FLWY) cleavage sites. Initial precursor and fragment mass tolerances were set at 10 and 20 ppm, respectively, and up to two missed cleavages were allowed for enzyme digestion. Cysteine carbamidomethylation was set as a fixed modification, and methionine oxidation, asparagine deamination were set as 'rare1' modifications. HCD and EThcd were chosen as the fragmentation types. Glycan modifications were searched against a the Byonic 'N-glycan 309 mammalian no sodium' library and were set as 'rare1' modifications. Two common modifications and one rare modification were allowed to be included per peptide. All other settings were set at the default values. For glycopeptides, a Byonic score of >300 was considered a good score, which reflects the absolute quality of the peptide-spectrum match [51]. The relative amount of each glycoform (%) was calculated by dividing the XIC peak area (obtained using Thermo Xcalibur 2.2) for each glycoform by the total glycoform peak area for that peptide and multiplying by 100.

Statistical analyses

All statistical analyses described were performed using GraphPad Prism 8.0. Data were assessed for normality before the selection of the appropriate test.

RESULTS

Deglycosylation identifies simple and hybrid glycans on the IBV S protein

Previous studies have identified glycosylation of the S protein of IBV, using insect cell-expressed M41 S proteins and a Vero cell-adapted Beaudette strain [5, 18, 19]. Here, the S protein of two strains of IBV were assessed, both propagated in chicken eggs to achieve a glycan profile reflecting that produced during infection in cells of the natural host. As a result of the oligosaccharide attachment and trimming processes that occur within the ER and Golgi during protein synthesis, different glycan forms can exist on each protein. Deglycosylation was achieved using two enzymes, PNGase F and EndoH. All glycans are susceptible to removal by PNGase F (bar alpha 1,3 linked fucose present in insect cells), as it cleaves at the GlcNAc core [52], whereas EndoH cleaves within the core of simple and hybrid glycans [53]. PNGase F and EndoH were used to begin characterisation of the glycan profile of the IBV S protein in the pathogenic M41-CK and the attenuated rIBV Beau-R, both members of the Massachusetts serotype and genotype GI-1 [54]. The presence of each type of glycan was indicated by sensitivity to enzymatic deglycosylation followed by a relative molecular mass shift measured by western blot. Different types of glycan were identified following digestion, as evidenced by the shift in S protein molecular weight following treatment with each reagent. As shown in Fig. 1, for both M41-CK (Fig. 1a) and Beau-R (Fig. 1b) the reduction in band size following PNGase F treatment indicates that a large proportion of the protein's apparent molecular weight is comprised of oligosaccharides. In the untreated samples, glycosylation is indicated by the band and smear at approximately 250 kDa, with the S2 band present at approximately 80 kDa. While glycans themselves do not exhibit a particularly heavy molecular weight, their branched nature renders glycosylated proteins bulkier than non-glycosylated proteins, hence they are perceived as larger or heavier when analysed by Western blot. The S protein's sensitivity to Endo H indicates that high mannose (simple/oligomannose and hybrid type) oligosaccharides contribute to a large proportion of its apparent overall molecular weight, indicated by the slightly larger band size compared to the PNGase F sample. This has been observed for other viral proteins such as HIV-1 gp120, in which 50% of the protein's apparent molecular weight is thought to be due to glycans on its surface [16].

An additional band is present in the Beau-R samples (Fig. 1b) compared to the M41-CK samples, approximately 37 kDa in size. This is thought to be a product of the S2′ cleavage site present in the Beau-R S protein [6]. Interestingly, this appears as a double band in the EndoH treated sample but only a single band is visible in the PNGase F sample, potentially a result of the complete deglycosylation by the latter enzyme. Nevertheless, there was a sizeable band shift following both treatments, indicating that a large proportion of the protein's apparent molecular weight can be attributed to glycan structures.

Predicted N-glycosylation site positions on the IBV S protein vary by strain

To explore glycosylation of the IBV S glycoprotein on a site-specific basis, the amino acid sequences of M41-CK, Beau-R, QX and 4/91 s proteins were analysed using the online server NetNGlyc 1.0, to identify any amino acid residues in the S protein sequences that were likely to be N-glycosylated. QX (genotype GI-19) and 4/91 (genotype GI-13) [54] display vastly different tropisms and *in vivo* phenotypes to the two laboratory strains, and each exhibit approximately 82%

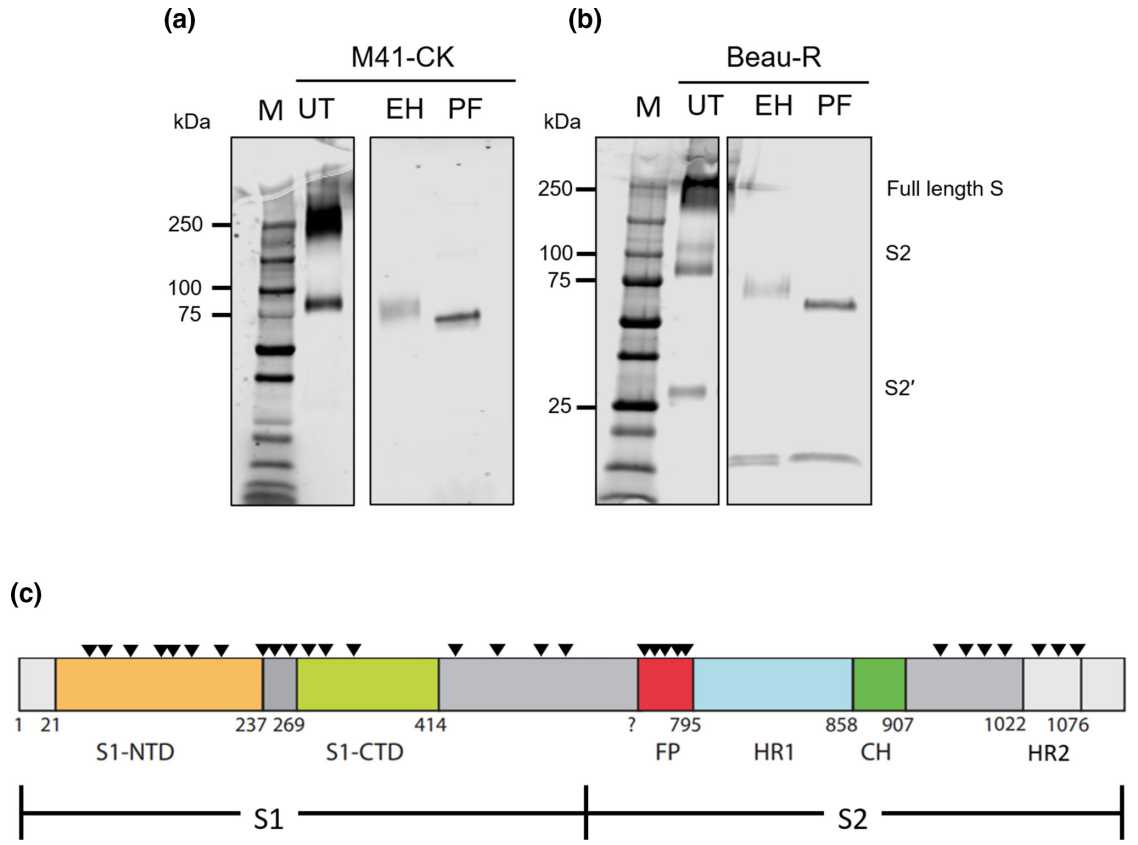

Fig. 1. IBV S is susceptible to enzymatic deglycosylation. Purified samples of IBV M41-CK (a) and Beau-R (b) were digested with EndoH (EH) or PNGase F (PF) for 1 h at 37 °C. Digested proteins were separated by SDS-PAGE followed by Western blot using the monoclonal IBV S2 antibody 26.1. Blots were visualized using a Licor Odyssey and band sizes (kDa) were compared to Bio-Rad All Blue Protein Standard (m). Digested protein samples were compared with untreated (UT) samples of purified virus for each strain. (c) Schematic representation of the S gene with predicted N-linked glycosylation sites indicated by black arrows. The locations of predicted sites for M41-CK and Beau-R are the same. Notable regions of the S protein are indicated in colour, NTD: N-terminal domain, CTD, C-terminal domain; FP, fusion peptide; HR, heptad repeat; CH, central helix. Amino acid numbers correspond to the amino acid sequence of IBV M41-CK S.

amino acid identity to both M41-CK and Beau-R. Both QX and 4/91 belong to their own serotypes and genotypes, again different from the Massachusetts serotype of M41-CK and Beau-R [55, 56], which have 96.2% amino acid identity in the spike protein. The locations of the predicted N-glycosylation motif, amino acid sequence N-X-S/T, were identified in four amino acid sequences representing the different IBV strains, M41-CK (GenBank accession number MK728875.1), Beau-R (GenBank accession number AJ311317), 4/91 (GenBank accession number JN192154) and QX (GenBank accession number DQ431199). The predicted locations of the N-linked glycosylation motif for each of the four IBV strains are indicated in Table 1.

There are similarities between the positions of the predicted N-glycosylation sites in each S protein of the four strains, with 26 sites shared across all strains. The positions of the predicted sites for M41-CK and Beau-R were identical, which is unsurprising due to the similarity (96%) of the two S protein sequences. Four additional predicted N-glycosylation sites are shared between QX and 4/91, with the most striking similarity within the S2 subunit. Two predicted N-glycosylation sites, at positions 141 and 200, are unique to QX, while 4/91 displays a single unique predicted site at position 281, all located within S1, which has the most variable amino acid sequences of the two subunits [57]. Given only a few differences exist between the predicted glycan profiles for the four strains described here, this may indicate that the glycosylation pattern of the S glycoprotein is largely conserved across IBV strains.

To assess the spatiality of these predicted sites in the M41-CK amino acid sequence, the locations were mapped to the predicted structure of the M41-CK S protein, based on the recently published M41 ectodomain structure, covering residues 21–1022 of the total 1162 residues in the M41 S amino acid sequence (Fig. 1c) [5]. M41-CK was selected for this analysis from the four strains described as Massachusetts is the most widely used vaccine serotype and is therefore of interest with relation to improving vaccine design [55, 58]. M41-CK is also pathogenic compared to Beau-R and is therefore a more clinically relevant strain for this analysis [59]. Fig. 2 shows a representation of the M41-CK S protein

Table 1. Predicted N-linked glycosylation site positions in the amino acid sequences of Beau-R, M41-CK, 4/91 and QX

		IBV Strain			
		Beau-R	**M41-CK**	**4/91**	**QX**
S1 SUBUNIT	S1-NTD	51	51	–	52
		–	–	54	55
		77	77	75	76
		103	103	103	104
		–	–	–	141
		144	144	146	147
		163	163	165	166
		178	178	180	181
		–	–	–	200
		212	212	214	215
		237	237	239	240
		247	247	249	250
		264	264	266	267
	S1-CTD	271	271	273	274
		276	276	278	279
		–	–	281	–
		306	306	308	309
	S2′→	425	425	427	428
		447	447	449	450
		–	–	456	457
		513	513	515	516
		530	530	533	533
S2 SUBUNIT		–	–	544	545
		579	579	581	582
		591	591	593	594
		669	669	671	672
		676	676	678	679
		714	714	–	–
		947	947	949	950
		960	960	962	963
		979	979	981	982
		1014	1014	1016	1017
	HR2	1038	1038	1040	1041
		1051	1051	1053	1054
		–	–	1060	1061
		1074	1074	1076	1077

Notable regions of the S protein are indicated on the left, including the S1 and S2 subunits, the S1 N-terminal domain (S1-NTD), S1 C-terminal domain (S1-CTD) and heptad repeat 2 (HR2). The S2′ cleavage site is indicated at position 690 (Beau-R). Numbers indicate the position of the asparagine (N) residue in the motif N-x-S/T and are numbered from the start codon of the signal sequence in each strain.

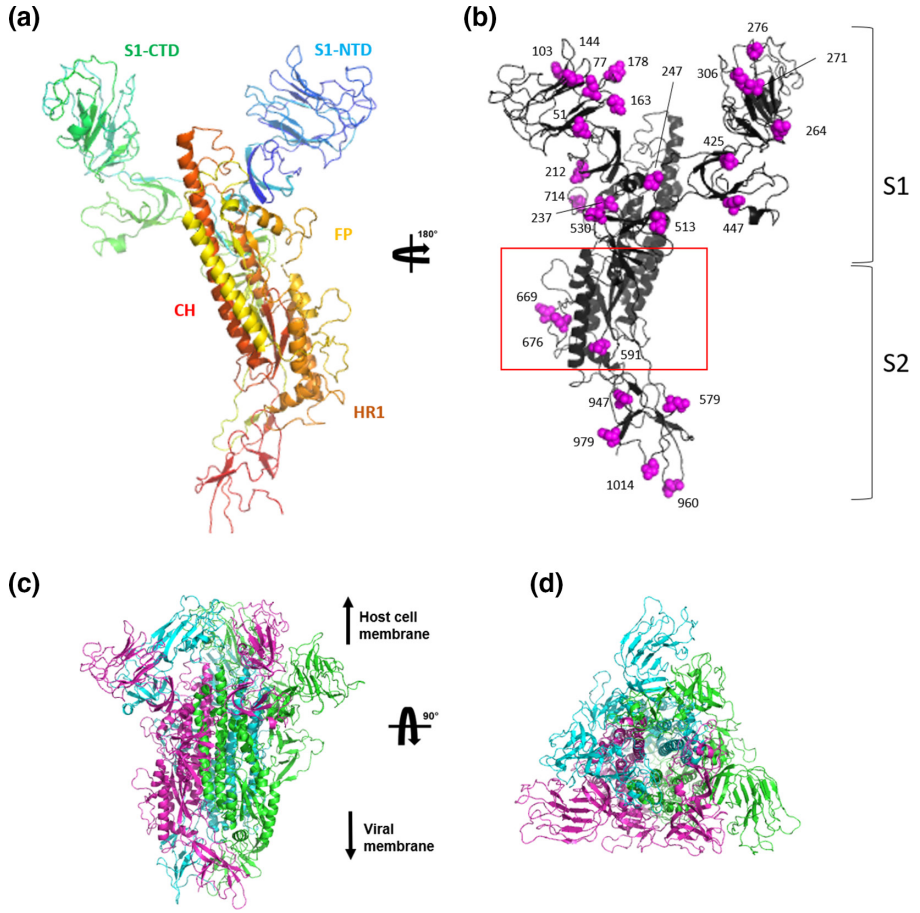

Fig. 2. Glycosylation is predicted at 29 sites in the M41-CK S protein sequence. Ribbon diagram of the putative S protein structure of IBV M41-CK. (a) Monomeric unit of the S protein coloured by rainbow from N (blue) to C terminus (red). S1 indicated in green/blue and S2 in red/yellow/orange. Functional domains are indicated. (b) Monomeric unit of the S protein with labelled Asn residues present in PNG sites (pink), generated using PyMol. Approximate location for binding of the monoclonal IBV S2 antibody 26.1 indicated by the red box (residues 546–725 [62]. (c) Trimeric formation of IBV M41-CK S from a side view and (d) from a top view, generated using SWISS Model. Each colour represents a monomeric unit.

structure with the predicted glycan sites labelled with spheres. The site locations listed in Table 1 correspond to the numbers detailed in Fig. 2(b). The NetNGlyc predictions identified 29 sites, which had the capacity for glycosylation. Of these predicted sites 18 lie in the S1 subunit and 11 in S2. The arrangement of three monomeric units within an M41-CK S protein trimer is shown in Fig. 2(c, d). None of the sites appeared to be facing inwards when analysed using PyMOL, however some were close to the start of the transmembrane domain around position 1096 in M41-CK.

Heterogeneity exists within the glycan profile of the M41-CK S protein

The prediction of glycosylation at a given asparagine residue is based on the presence of the N-X-S/T motif, but the likelihood of a glycan being attached to the predicted residue depends on multiple factors, such as the amino acids surrounding the motif [20]. To determine whether the predicted sites highlighted in Fig. 2 were utilized in the M41-CK S sequence, with a glycan structure attached to the asparagine residues, a sample of ultracentrifuge-purified virus propagated in embryonated hens' eggs was trypsin and chymotrypsin digested and analysed using mass spectrometry (MS). This resulted in coverage of the M41-CK S protein as multiple peptides, as indicated in Fig. S1 (available in the online version of this article). Analysis of the 29 predicted N-glycosylation sites by MS, confirmed glycan presence at 18 sites by MS and furthermore the composition of the glycan structures was analysed at eight of these 18 sites using EThcD MS techniques, detailed in Fig. 3, allowing further insight into the types of glycan present at these sites. Of the 18 confirmed sites, nine are present in the S1 subunit and nine in S2, with four sites present in the S1-NTD receptor binding domain at N77, N103, N144 and N212 [5, 60].

The oligosaccharide compositions of the glycan structures were characterised by EThcD at amino acid sites N144, N212, N425, N513 in the S1 subunit and N947 and N1014 in the

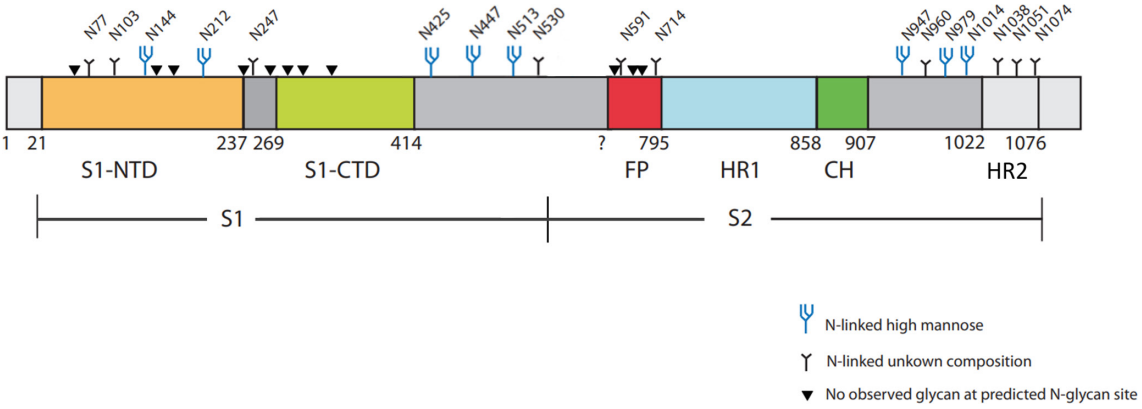

Fig. 3. Heterogeneity exists in the glycosylation profile of M41-CK S protein. Schematic representation of the M41-CK S gene with functional domains and amino acid positions indicated. NTD: N-terminal domain, CTD: C-terminal domain, FP: fusion peptide, HR: heptad repeat, CH: central helix. In samples of ultracentrifuge-purified samples of IBV M41-CK, glycan sites were mapped by trypsin or chymotrypsin digestion followed by PNGase treatment in presence of D_2O. Glycopeptides (trypsin and chymotrypsin digests) were analysed on Thermo Orbitrap fusion instrument (ETHcD mode). To visualize the predicted structure of the glycans, glycopeptide MS data were analysed with Byonic software (Protein Metrics). The presence of N-linked high mannose glycans is indicated by a blue structure at sites N144, N212, N425, N447, N513, N947, N979 and N1014 (analysed using Byonic). The presence of glycans of an unknown structure is indicated by black markers at sites N77, N103, N247, N530, N591, N714, N960, N1038, N1051, N1074. Sites at which N-glycosylation was predicted by NetNGlyc 1.0 but not confirmed during mass spectrometry analyses are indicated by black arrows.

S2 subunit. At all of these sites, the structures appeared to be oligomannose-type glycans, with some variation between the composition of mannose molecules in the glycan chains. Heterogeneity among the glycan-types present was observed at N144, N212, N425, N513 and N947. The relative glycan compositions at each site are detailed in Table 2.

This heterogeneity within the range of structures identified at these sites indicates that the structures may differ on the individual S proteins within the sample. Due to the preparation and digestion methods, approximately 50% coverage of the S protein was achieved in these experiments, so this list may not be exhaustive. These results do, however, prove that these sites are true glycosylation sites and are occupied by glycan structures. Combined, the results from the MS experiments demonstrate a high level of glycosylation site usage in the IBV S protein, as previously described, and allude to heterogeneity in the range of glycan types and structures present at each site on individual S proteins.

Monoclonal antibody recognition is altered following treatment with kifunensine

Complex glycans are also present on the S protein, as indicated by the effects of the mannosidase inhibitor kifunensine (Fig. 4). Kifunensine is a cellular inhibitor of α-mannosidase I, preventing the trimming of precursor glycoproteins and the removal of mannose molecules [61]. This leaves glycans in high mannose states and reduces the quantity of complex glycans formed in the Golgi following protein modification in the ER [61]. The inhibition of complex glycan formation by kifunensine on the IBV S glycoprotein was analysed using confocal microscopy by identifying any changes in antibody recognition following treatment with kifunensine. Monoclonal antibody (mAb) 26.1 is known to bind somewhere between amino acid residues 546 and 725 within the S2 subunit [62]. This antibody was selected for this analysis as it was readily available and compatible with both Western blot and immunofluorescence techniques, unlike others in the limited selection of available reagents for IBV. As can be seen from Fig. 4(a), there was no difference in recognition of M41-CK S2 by mAb 26.1 after treatment with kifunensine in CK cells. However, analysis of CK cells infected with Beau-R identified that there was a substantial decrease in the presence of S2 signal in the cells treated with kifunensine at the time of infection (Fig. 4a), indicating that the inhibition of complex glycan formation had altered how the Beau-R S protein was recognized by the antibody. This was repeated for Beau-R in the continuous cell line DF-1 cells, where the same effect was observed (Fig. 4b). M41-CK was not included in these analyses as it cannot be propagated in continuous cell lines [8]. This demonstrates that the effects of kifunensine on the recognition of Beau-R S2 by mAb 26.1 are not unique to primary CK cells, indicating the effect is not cell specific. Detection of IBV S2 was also measured by Western blot analysis using IBV-infected CK cell lysates (Fig. 4c). IBV S2 was detected in both untreated (UT) and kifunensine-treated samples of CK cells infected with M41-CK or Beau-R. A subtle change was observed in the amounts of S2 detected in CK cells infected with M41-CK or Beau-R S2 following kifunensine treatment; slightly less S2 was detected following treatment with kifunensine and interestingly the S2 subunits appeared larger when compared to the untreated samples. Levels of β-actin remained unchanged following kifunensine treatment, indicating that there were no adverse cellular effects from the concentration of the inhibitor used. This was

Table 2. N-glycosylation in the IBV M41-CK S glycoprotein and relative glycoform abundance (%) at each site

N-glycan site									
		Predicted	Observed						
Subunit	**Domain**	**Position**	**HCDpdEThcd**	**D_2O labelled**	**Enzyme**	**Peptide sequence**	**Glycan composition**	**Relative glycan composition (%)**	**Glycan type**
S1	S1-NTD	144	144	144	Chymotrypsin	Y.NLTVSVAKYPTF.K	HexNAc(2)Hex(7); HexNAc(2)Hex(8)	74;26	N-linked oligomannose
S1	S1-NTD	212	212	212	Trypsin	K.ALAYFVNGTAQDVILCDGSPR.G	HexNAc(2)Hex(8); HexNAc(2)Hex(9)	26;74	N-linked oligomannose
S1		425	425		Trypsin	R.HNYNNITLNTCVDYNIYGR.T	HexNAc(2)Hex(5); HexNAc(2)Hex(6); HexNAc(2)Hex(7); HexNAc(2)Hex(8)	23;17;27;33	N-linked oligomannose
S1		447	447	447	Chymotrypsin	Y.GRTGQGFITNVTDSAVSY.N	HexNAc(2)Hex(8)	100	N-linked oligomannose
S1		513	513	513	Trypsin	R.NETGSQLLENQFYIK.I	HexNAc(2)Hex(5); HexNAc(2)Hex(7); HexNAc(2)Hex(8)	37;37;26	N-linked oligomannose
S2		947	947	947	Chymotrypsin	F.SYTPDSFVNVTAIVGF.C	HexNAc(2)Hex(5); HexNAc(2)Hex(7); HexNAc(3)Hex(6)	46;24;30	N-linked oligomannose
S2		979	979	979	Chymotrypsin	F.IQVNGSYY.I	HexNAc(2)Hex(5)	100	N-linked oligomannose
S2		1014	1014	1014	Chymotrypsin; Trypsin	Y.VSVNKTVITTF.V; R.AITAGDIVTLTSCQANYVSVNK.T	HexNAc(2)Hex(5)	100	N-linked oligomannose

Position refers to asparagine residue position in the amino acid sequence of IBV M41-CK S protein. Blank cells indicate that the glycan was not confirmed by this method.

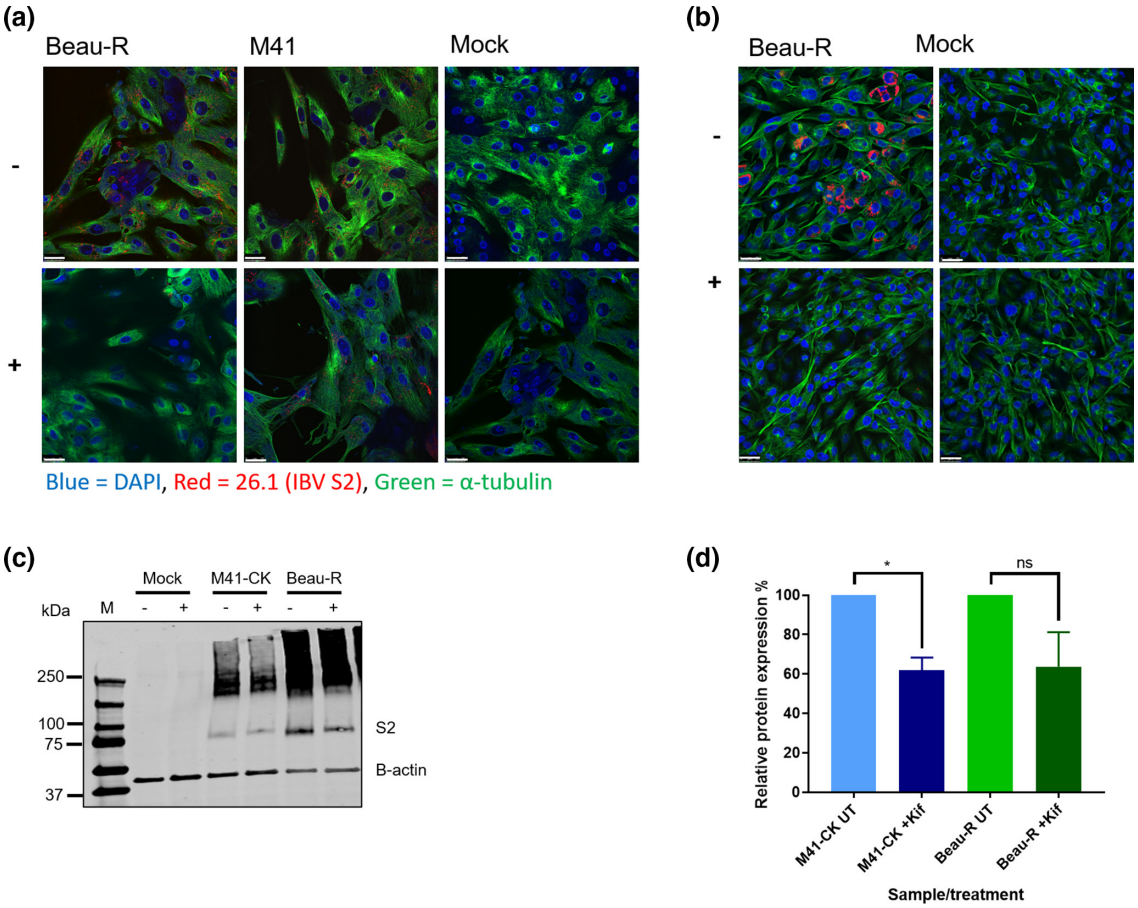

Fig. 4. Complex glycosylation influences recognition of IBV S2 by monoclonal antibody. (a) CK cells were infected with M41-CK or Beau-R (m.o.i.=1) and treated with kifunensine (20 µm) at the time of infection. After 24 h, cells were fixed and stained using monoclonal antibodies against IBV S2 (26.1, red) and α-tubulin (green). Nuclei were stained with DAPI (blue). Cells were assessed by confocal microscopy. Untreated cells (-) were compared with kifunensine treated cells (+) and mock-infected cells. White scale bars indicate 25 µm. (b) DF-1 cells were infected with Beau-R (m.o.i.=1) and treated with kifunensine at the time of infection. Cells were fixed and stained as described and compared to mock-infected cells. (c) CK cell lysates were prepared from mock- or IBV-infected cells and separated by SDS-PAGE. IBV S2 was detected using monoclonal antibody 26.1, producing bands of approximately 80 kDa. B-actin was used as a cellular loading control, producing bands at approximately 42 kDa. Band sizes were compared for mock-, M41-CK- and Beau-R-infected samples between untreated (-) and kifunensine-treated (+) cells. Sizes were determined in kDa using Bio-Rad All Blue Protein Standards (m). (d) Densitometry data was generated from three independent infections and Western blots using the Licor Odyssey quantification function. Relative protein expression levels for M41-CK S2 and Beau-R S2 are shown, with kifunensine-treated samples (+Kif) displayed as a percentage value of expression levels in the untreated (UT) samples. Average values are displayed with SEM. Data were analysed by *t*-test for each strain and statistical differences are indicated, where * indicates P <0.02.

also confirmed by assessment of cell viability using Promega CellTiter-Glo (data not shown).

To quantify any differences in expression or detection by Western blot analysis, the densitometry of each band was analysed and compared. Fig. 4(d) shows the densitometry data of the kifunensine-treated samples, normalized to β-actin levels and displayed as a percentage of the S2 expression in the untreated samples. There was a significant reduction in S2 expression for M41-CK (P <0.02) but not Beau-R, even though levels of S2 in both samples reduced by nearly 40% on average following treatment with kifunensine. This indicates that there was some negative effect on either expression of the S protein or detection of S2 by mAb 26.1. As an inhibitor of α-mannosidase I, kifunensine interferes with the regulation of protein folding in the ER [14]. The lower levels of S2 in the kifunensine-treated samples may indicate a change in folding of the S protein and subsequently loss or distortion of epitopes required for antibody binding. By homogenizing the glycan types present on the surface of the S protein, kifunensine may have induced a denser glycan shield, which may have also contributed to blocking recognition by increased shielding of the antibody epitope. In addition, there could also be effects on the function of the S protein in the absence of complex glycosylation, reducing the binding ability of the protein and hence entry into target cells.

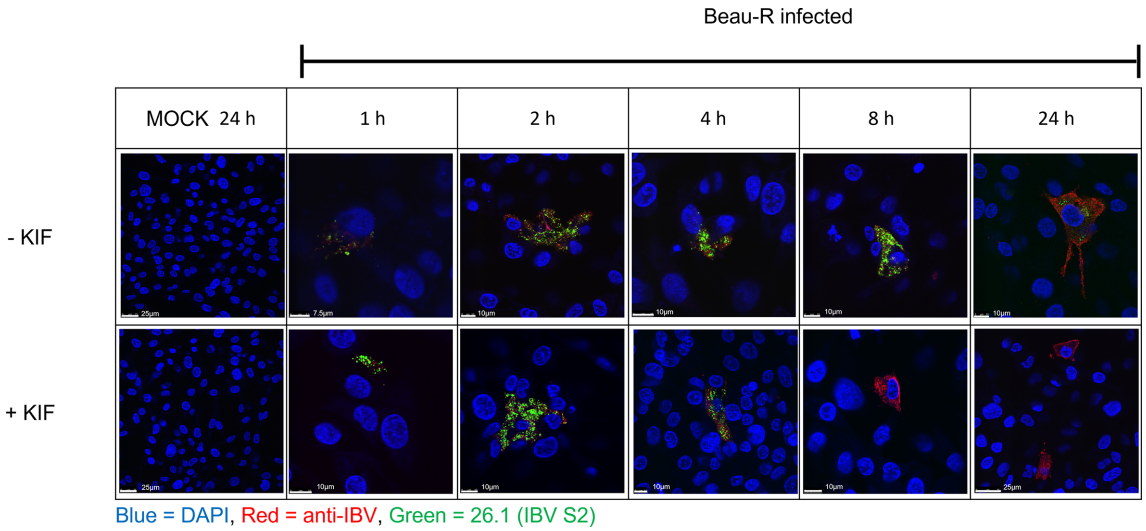

Fig. 5. Kifunensine causes a loss of Beau-R S2 recognition between 4 and 8 h p.i. DF-1 cells were infected with Beau-R (m.o.i.=10), treated with kifunensine at the time of infection and incubated at 37 °C. Infected cells were fixed at 1, 2, 4, 8 and 24 h p.i. and mock-infected cells were fixed at 24 h p.i. only. Cells were stained with the monoclonal S2 antibody 26.1 (green) and the polyclonal IBV antibody anti-IBV (red). Nuclei were stained with DAPI. Cells were assessed by confocal microscopy and images are displayed for untreated (-KIF) and kifunensine-treated (+KIF) cells. Staining for both antibodies was visible until 4 h.p.i., after which only anti-IBV staining was visible in the kifunensine-treated samples. Scale bars are indicated in white for each panel.

Kifunensine affects antibody recognition late in Beau-R infection

The results from the inhibition of complex glycan formation by treatment with kifunensine indicated an effect on Beau-R S2 recognition by mAb 26.1 following detection by confocal microscopy (Fig. 4a, b). To determine the stage, during infection, at which this effect becomes apparent DF-1 cells were infected with Beau-R, treated with kifunensine at the point of infection, fixed at 1, 2, 4, 8, and 24 h post-infection (p.i.) and analysed by confocal microscopy using the S2 mAb 26.1. In addition, Beau-R infected DF-1 cells were also analysed using the polyclonal antibody anti-IBV (chIBV), which recognizes IBV (Massachusetts) proteins (Abcam). DF-1 cells were chosen for these analyses as the images obtained during staining are generally clearer compared to primary CK cells. As can be seen from Fig. 5, in the absence of kifunensine, the Beau-R S2 protein was detected at all time points using either antibody, indicating that the cells were infected, albeit to a low level, and that S2 was detectable in its untreated form. In the kifunensine-treated samples, both antibodies detected Beau-R S2 at the earlier time points of 1, 2 and 4 h p.i. indicating Beau-R had entered the cells and initiated a replication cycle. However, from 8 h p.i. the detection of Beau-R S2 using mAb 26.1 was lost completely, whereas the detection of S2 using chIBV was present at all time points including 8 and 24 h p.i. These observations indicate that infection with Beau-R was still viable, following treatment with kifunensine, even though S2 was not detectable by mAb 26.1. The data implies that the effects of kifunensine treatment take place between 4 and 8 h p.i. The replication cycle of IBV is considered to be 6–8 h, with virus progeny detectable at 6 h p.i. [63]. Our data indicates that kifunensine is acting on the newly produced proteins, rather than those present on virions in the starting inoculum and that kifunensine treatment affects detection of Beau-R S2 by mAb 26.1 for confocal microscopy. This presents a dichotomy with the data described for Western blot analysis, where Beau-R S detection was reduced but not abolished following kifunensine treatment. This is hypothesized to be because kifunensine changes the final conformation of the S protein to a degree where it is no longer recognized by mAb 26.1, but the linear epitope is still recognized during Western blot analysis, even though a reduced amount is detected overall.

Complex glycans are non-essential in Beau-R and M41-CK replication

To further investigate the potential effects of kifunensine treatment on IBV infection, cell supernatants from CK cells infected with IBV (m.o.i.=1) and treated with kifunensine, were titrated on CK cells to identify any changes in viral titres following kifunensine treatment in comparison to untreated controls (Fig. 6a). No significant differences in viral titres were observed for either Beau-R or M41-CK at 24 h p.i. There was a small reduction in titres of Beau-R propagated in the presence of kifunensine, however, this did not reach statistical significance. The comparable titres of both Beau-R and M41-CK propagated in the presence and absence of kifunensine indicate that the inhibition of α-mannosidase I and consequently the formation of complex glycans on the S protein, does not affect either Beau-R or M41-CK viability and infectivity. To confirm that other viral proteins were not affected by the actions of kifunensine, the envelope (E) protein was detected by western blot from IBV-infected CK cell lysates, using a monoclonal antibody against the E protein (Fig. 6b). In both

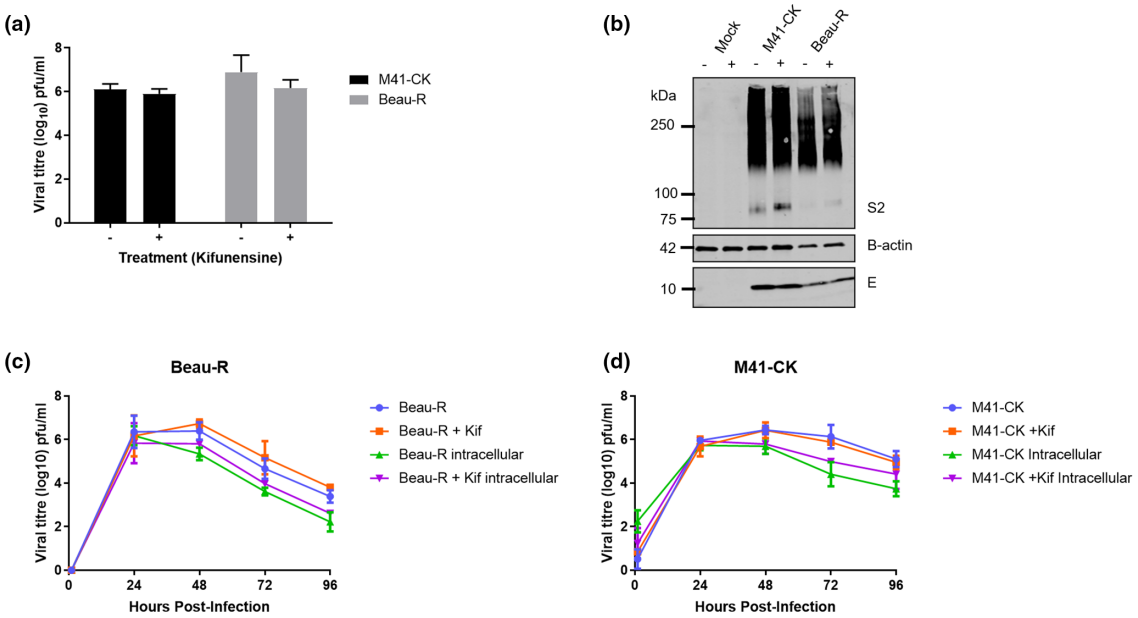

Fig. 6. Complex glycosylation is non-essential for IBV replication. (a) CK cells were infected with M41-CK or Beau-R, treated with kifunensine at the time of infection, and incubated at 37 °C. Supernatant was harvested at 24 h p.i. and titrated by plaque assay in CK cells. Average viral titres (log_{10} pfu/ml) from three independent experiments are displayed for untreated (-) and kifunensine-treated (+) cells infected with each strain. Error bars represent SEM and data were analysed by one-way ANOVA to identify statistical differences. (b) CK cell lysates from the infections described were prepared and separated by SDS-PAGE followed by Western blot using IBV-specific mAbs anti-S2 (26.1) and anti-E. Anti-B-actin was used as a loading control. Band sizes (kDa) were compared to Bio-Rad All Blue Protein Standards and untreated (-) samples were compared with kifunensine-treated (+) samples. (c) CK cells were infected with Beau-R or (d) M41-CK at an m.o.i. of 0.01 and treated with kifunensine at the time of infection. Cells were incubated at 37 °C. Supernatant and cell lysates were harvested at 1, 24, 48, 72 and 96 h p.i. and titrated by plaque assay in CK cells. Average viral titres from three independent experiments are displayed with SEM. Data were analysed by two-way ANOVA to identify statistical differences. Values for cell lysate samples are labelled intracellular and kifunensine treatment is indicated.

untreated and kifunensine-treated samples, the E protein was detected at 24 h p.i., with no size difference observed in either sample, indicating that there is no adverse effect on the E protein by kifunensine treatment. The E protein does not display N-glycans and so should not have been affected by the inhibition of α-mannosidase I [64].

The ER and Golgi play an important role in the secretory pathway, trafficking viral proteins to the cell surface during assembly and release [65]. As α-mannosidase I is an enzyme located in the ER, it was hypothesized that the inhibition of this enzyme by kifunensine and consequent loss of complex glycans, may interfere with the production of viable proteins for assembly into functional virions, potentially impacting virus release from infected cells and the concomitant increase in virus particles within infected cells. To test this hypothesis, replication kinetics of M41-CK and Beau-R were assessed in CK cells infected at a low m.o.i. (0.01) in the presence and absence of kifunensine (20 µm, added at the time of infection). Supernatants (extracellular) and cell lysates (intracellular), from five time points post-infection, were titrated on CK cells to determine the quantities of infectious virus progeny (Fig. 6c, d). No differences in titres between the untreated and kifunensine-treated samples for either Beau-R or M41-CK were observed, further indicating that complex glycans are not essential for replication of IBV in CK cells. There were no significant differences between the intracellular and extracellular titres, indicating that inhibition of α-mannosidase I by kifunensine did not impact on the ability of the virus to exit cells during replication.

Complex glycosylation is not required for *in vitro* virus neutralisation

Previous HIV-1 research has shown that some antibodies recognize the conformation of a protein including complex glycan structures [28, 32]. Neutralization of IBV by monoclonal antibodies raised against the S1 subunit of the IBV S glycoprotein has been described, including the mAb A13 for which neutralization is specific to M41 so does not neutralize Beau-R [47]. The anti-S2 mAb, 26.1, used in the previous experiments (Figs 1 and 4–6) is not neutralizing to either M41-CK or Beau-R. To assess whether M41-CK propagated in the presence of kifunensine exhibited an altered neutralisation response to treatment with the S1 mAb A13, a plaque reduction assay was performed in primary CK cells to determine the plaque reduction neutralization titre ($PRNT_{50}$) (Fig. 7a). The rIBV Beau-R was included in the assay to determine whether treatment with kifunensine would result in mAb A13 mediated neutralization. No significant differences

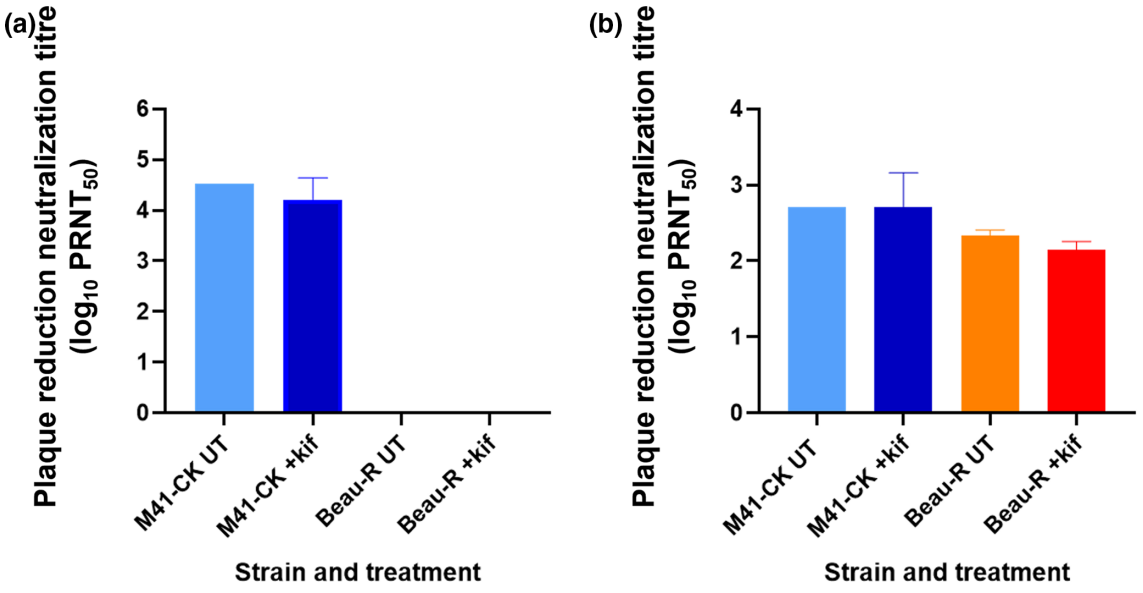

Fig. 7. Treatment with kifunensine does not affect neutralization by monoclonal antibody. Samples of supernatant from untreated (UT) and kifunensine-treated (+kif) M41-CK and Beau-R infected CK cells were diluted to 2000 p.f.u. and incubated with serial dilutions of monoclonal IBV S1 antibody A13 [47] (a) and polyclonal chicken sera raised against M41-CK (b). Virus-antibody solutions were titrated by plaque assay in CK cells and the plaque reduction neutralization titre ($PRNT_{50}$) was determined for each sample using the Reed-Muench calculation. $PRNT_{50}$ values from three independent experiments are displayed with SEM. Data were analysed by one-way ANOVA to identify statistical differences.

were observed between the $PRNT_{50}$ values for mAb A13 on M41-CK grown in the presence or absence of kifunensine (Fig. 7a). There was a slight decrease in the neutralization titre in the kifunensine-treated sample; this, however, was not statistically significant. The comparable titres therefore indicated that the recognition and neutralization of M41-CK S1 by mAb A13 is not dependent on the presence of complex glycans. As previously described for Beau-R [47], A13 was not neutralizing and this was unchanged following treatment with kifunensine (Fig. 7a). This implies that the neutralising effect of mAb A13 is not dependent on complex glycans on the M41-CK S glycoprotein, and is dependent on either the primary amino acid sequence of the protein or a specific conformation of the M41-CK S protein.

The mAb A13 recognises a small section of the S protein, within hypervariable region 1 (HVR-1) [47]. Following the result that kifunensine treatment does not affect the neutralization of M41-CK by mAb A13, plaque reduction assays were repeated but using polyclonal sera raised against M41-CK in chickens [48], to establish the effect of kifunensine treatment on virus neutralization (Fig. 7b). As both viruses belong to the same serotype, it was hypothesized that neutralization may be observed for both M41-CK and Beau-R, hence both strains were included in the assay. For polyclonal sera, similarly to the mAb A13 results, there were no differences in $PRNT_{50}$ values following treatment with kifunensine (Fig. 7b). However, both viruses were neutralized by the polyclonal sera, with the sera showing a stronger neutralization towards M41-CK than to Beau-R. Treatment with kifunensine had no effect on neutralization, although the titres were slightly decreased for Beau-R in the presence of kifunensine. Overall, the $PRNT_{50}$ values for M41-CK and Beau-R were similar. There was also slightly more variation within the titres obtained for the M41-CK kifunensine-treated samples, but the differences were not of statistical significance. Taken together these results indicate that complex glycans do not play an essential role in the neutralization of M41-CK or Beau-R *in vitro*, by mAb A13 or polyclonal sera.

DISCUSSION

The glycosylation of virus structural proteins has been shown to influence many of the processes and outcomes of a virus infection, including antigenicity, infectivity and receptor binding [18, 19, 37, 66–68]. The glycan profile is an important factor to consider when investigating how a virus interacts with a cell and how the glycan shield may aid in immune evasion and affect antibody recognition. Recent studies using the S glycoprotein of SARS-CoV-2 suggested that 40% of the protein's surface is covered by glycans, reducing the surface of the protein accessible to antibody recognition [69, 70]. This is in line with data from other heavily glycosylated virus proteins, such as HIV-1 gp120 where 50% of the protein's apparent molecular weight was attributed to glycosylation [23], with the glycan profile comprising oligomannose, complex and hybrid glycans [71]. The abundance of glycans present on the IBV S protein was initially investigated, in this study, using enzymatic deglycosylation, which revealed a decrease in the

relative molecular mass of the S protein and S2 subunit by Western blot analysis. Further investigation, using EndoH, identified a molecular weight change suggesting that the glycan shield of the M41-CK and Beau-R S proteins contain both simple and hybrid glycans (Fig. 1a, b). Investigations using kifunensine revealed the presence of complex glycans (Fig. 4). The identification of several types of glycan in the glycan shields of both Beau-R and M41-CK suggest diversity in the glycans present on the S glycoprotein.

Sequence analysis of four different strains of IBV, spanning three genotypes [54] and three serotypes [1, 55], showed small differences in the numbers of predicted glycosylation sites within the S protein (Table 1), with 29 sites predicted in M41-CK and Beau-R, 32 in 4/91 and 34 in QX, as previously reported [24]. These numbers are broadly similar to those reported for other coronaviruses such as human coronavirus 229E, which possesses 30 predicted sites in its S protein [72] and feline infectious peritonitis virus which has 37 [73]. The predicted glycosylation sites were identical for M41-CK and Beau-R, which was not unexpected given the high level of amino acid identity between the two strains, and that both belong to the same serotype. Using purified virus stocks derived from propagation of M41-CK in embryonated eggs, we were able to confirm glycosylation at 18 of the 29 predicted glycosylation sites in the M41-CK S protein (Fig. 3), seven of which matched those identified by Zheng *et al.* [18], following expression of the Vero-adapted Beaudette S protein in insect cells. The location of one site identified by Zheng *et al.* [18], at position N276, was not covered by the peptides detected in the present study, and so glycosylation was not confirmed.

Glycans were also identified at 20 sites in the M41 S protein as part of the cryo-EM structural analyses performed by Shang *et al.* in 2018, although this study used insect cell expression systems. Ten of these sites aligned with those confirmed here in M41-CK, possibly as a result of the difference in expression systems [27]. Differences were also noted in another study investigating glycosylation in the M41 RBD, which analysed ten predicted sites using LC/MS and MALDI-TOF MS techniques [19]. Although this study also used an M41 isolate of IBV, the sites identified did not match those identified in this study using M41-CK. There were differences in amino acid positions and sequences for those that were identified by Parsons *et al.* [19] compared with those in the present study. There were also differences in the observed glycoforms in each study, with Parsons *et al.* describing complex-type glycans compared to the oligomannose types described here. The differences between the results obtained in each of these IBV M41 glycosylation studies highlight the impact of the expression method for the S protein and cell type for propagation of virus on the glycan profile of the viral proteins, as well as reiterating the importance of expressing intact trimers in glycosylation investigations. This was also observed in studies using HIV-1, where differential glycosylation was observed between different mammalian cell types [74], and for influenza virus, where differences in HA glycosylation was dependent on growth in mammalian or avian cells [27]. The experiments described here, using IBVs propagated in embryonated hen's eggs or chicken cells, offer a description of IBV glycosylation more comparable to infection in the natural host.

The structures of the glycans present at six of the confirmed sites in the M41-CK S protein were also determined using the EThcD MS techniques. Notably, a degree of heterogeneity was observed in the glycan structures observed at these sites (Table 2). This has recently been reported for the S protein of the newly emerged SARS-CoV-2, where structural analyses and simulations suggested that while the antigenicity of the S protein is unlikely to be affected by heterogeneity, there may be implications for the presentation of specific epitopes [70]. Glycan heterogeneity has been identified in the envelope (Env) protein of HIV-1, where it was linked to immune evasion [75, 76], offering important insights into how these viruses may evade immune responses. However, it is important to note that while glycans do shield some HIV epitopes from antibody recognition, there is also homogeneity at certain sites in the glycan shield of HIV Env, which renders the protein susceptible to broadly neutralizing antibodies that recognize specific glycans [32, 77]. The cause of the heterogeneity observed for IBV M41-CK S is likely to be multifactorial. It could be due to more than one cell type being infected within the embryo, as the specific site of IBV replication within an egg is unknown. As there may be more than one cell type infected, it would be difficult to say which cell types have resulted in which variations. Furthermore, the metabolic activity and enzyme repertoire of each of these cell types are also likely to impact glycosylation [78].

The effects of glycosylation on antibody recognition have been documented for viruses including HIV-1 and influenza [68, 74, 79]. The results described in Fig. 4 also indicate an effect of complex glycosylation on antibody recognition during both Beau-R and M41-CK infection. Levels of detected spike protein, as measured by Western blot, were shown to decrease following treatment with kifunensine for both M41-CK and Beau-R, but the protein was still recognized by the mAb 26.1, targeting the S2 subunit (Fig. 4c, d) [62]. In contrast, when analysed by confocal microscopy, the signal from the S2 26.1 mAb was completely lost in the Beau-R infected cells treated with kifunensine after 24 h. (Fig. 4a, b). This indicates that the effect is only observed when the antibody is interacting with the conformational form of the S protein, as the linear epitope was still recognized following Western blot analysis, although a reduction in detection levels was noted following kifunensine treatment (Fig. 4c, d). As kifunensine inhibits α-mannosidase I, which regulates protein folding in the ER, it is likely that the action of the inhibitor, and the disruption of complex glycosylation during protein synthesis, has resulted in a different conformational form of the protein, unrecognised by the mAb 26.1. There may also be an increased shielding effect in the kifunensine-treated samples, where the glycan shield may be more dense following treatment as a result of the composition of the remaining glycans, potentially blocking access to epitopes on the surface of the S protein. Interestingly, this effect was also strain-specific, with M41-CK-infected cells seemingly unaffected by treatment with kifunensine. This

could indicate that complex glycosylation is less important in the folding of M41-CK S proteins, or that mAb 26.1 recognizes the protein differently with this strain. The mAb 26.1 binds at residues 546–725 [62] in the M41 S protein sequence, a region possessing five predicted glycosylation sites in both M41-CK and Beau-R, two of which were confirmed in M41-CK. As there was no difference in recognition for M41-CK by immunofluorescence, perhaps the glycans on the Beau-R spike protein are complex in type and those on M41-CK are simple glycans, for example. Equally it is possible that the Beau-R epitope targeted by mAb 26.1 has been distorted as a result of aberrant processing with the inhibition of mannosidase I. Further investigation into the change in recognition of Beau-R S2 revealed a more specific time at which the loss of signal was observed (Fig. 5), between 4 and 8 h p.i., which aligns with one round of IBV replication [63]. As kifunensine inhibits a cellular enzyme, it is therefore likely that it starts to take effect on the newly synthesized proteins during virus replication. Complex glycans have been implicated in the recognition of HIV-1 glycoproteins by broadly neutralizing antibodies [28] and dependency on glycans and glycosylation in antibody binding has been noted for other viruses including HIV-1 and influenza [31, 80–82], supporting the data described here for recognition of IBV Beau-R S. These data suggest the presence of glycan-dependent epitopes on the surface of the IBV S protein.

Our results indicate that neutralization of IBV infectivity is not solely dependent on complex glycans, despite the indication of glycan-dependent epitopes on the surface of the S protein. The neutralizing capacity of a mAb (26.1) and polyclonal chicken sera was the same when neutralizing wild-type IBV and IBV produced in kifunensine-treated cells, i.e. those without complex glycans, indicating that complex glycosylation does not affect neutralisation of M41-CK or Beau-R by mAb A13 or polyclonal anti-M41-CK sera (Fig. 7). This contrasts with HIV-1 studies, where treatment with kifunensine increased susceptibility to neutralization by sera [14], presumably through disruption of the glycan shield. Although there was a slight increase in serum neutralization titre in the M41-CK kifunensine-treated samples, the difference was not significant (Fig. 7b). Removal of complex glycans from the surface of the Beau-R S protein had no effect on its susceptibility to neutralisation by the mAb A13, in line with previously published data [27]. The effect described here may be antibody-specific, and further investigation would be required to assess the effect with other antibodies. Changes in glycosylation patterns in recombinant proteins have also been shown to alter serum neutralization titres during *in vivo* experiments [83] and so, although no change was observed using polyclonal sera *in vitro*, viruses or vaccines lacking complex glycans may display altered phenotypes or antibody responses in infected birds.

Glycosylation of the S protein has been reported to affect receptor binding in other IBV studies [19], and it was hypothesized that the removal of complex glycans may affect entry and/or exit from host cells. However, our results (Fig. 6) show that the presence of complex glycans did not appear to affect virus infectivity. Kifunensine treatment exerted no effect on the replication or release of IBV in infected cells, where the titres of intra- and extracellular viral progeny were comparable at all time points following treatment with kifunensine. A more subtle effect was observed in the Western blot experiments detecting the S protein (Figs 4c and 6b), where a very slight size increase was observed in the S2 bands from kifunensine treated samples, observed across multiple independent experiments. This is surprising as the inhibition of glycosylation usually reduces the relative molecular mass of a protein [84], although this is dependent on the size of the glycans inhibited and that of those remaining. The increase in size may be due to the reduced activity of α-mannosidase I, which aids in adding and removing residues from developing glycan structures [15]. The glycans on this subunit may not be properly trimmed, and so exhibit a slightly heavier weight compared to proteins produced in untreated cells. However, as described, no effect was observed in relation to replication, with titres of viral progeny in the kifunensine-treated samples comparable with the untreated, indicating that these IBV strains were functional without complex glycans.

Taken together the results described here highlight a notable interaction between complex glycosylation and the recognition of the IBV S protein by a monoclonal S2 antibody, with no impact on virus replication, infectivity or neutralisation by polyclonal sera. Different types of glycan have been identified in the spike proteins of M41-CK and Beau-R, with the importance of certain types differing between the strains. We have shown that the majority of predicted glycosylation sites in the M41-CK S protein are utilized and that heterogeneity exists within the range of glycans present at each position. This research explores the basic principles of glycosylation in the IBV spike protein, and with effects observed surrounding the recognition of the S protein by antibodies, this may be useful to incorporate into vaccine design. As suggested for HIV-1 vaccination strategies, the generation of immunogens capable of inducing broadly neutralizing antibodies, which recognize the glycan shield would be highly beneficial [28]. The results from the experiments described here showed no change in neutralization following complex glycan removal, but there was clearly an alteration in the mechanism of antibody binding to the S2 subunit, which is more conserved among IBV strains than the variable S1. Further research is required to establish whether IBV S proteins lacking glycans are able to induce more broadly cross-reactive antibodies upon vaccination against IBV.

Funding information
This research was funded by UKRI Biotechnology and Biological Sciences Research Council (BBSRC) grants BB/R019576/1, BBS/E/I/00001977 and BBS/E/I/00007034.

Acknowledgements
Thanks to Dr Simon Spiro for kindly gifting the initial stocks of kifunensine. Thanks also to Dr Tom Peacock for assistance with the sequence analysis of the N-glycosylation sites in the S protein sequences.

Author contributions

Conceptualization, P.B., E.B. and P.S.L; methodology, P.S.L., S.K. and S.A.; validation, P.S.L., S.K. and S.A., formal analysis, P.S.L. and S.A.; investigation, P.S.L. and S.K.; writing–original draft preparation, P.S.L.; writing–review and editing, S.K., P.B., S.A. and E.B.; supervision, P.B. and E.B.; funding acquisition, E.B. All authors have read and agreed to the published version of the manuscript.

Conflicts of interest

The authors declare that there are no conflicts of interests.

References

1. Cook JK, Jackwood M, Jones RC. The long view: 40 years of infectious bronchitis research. *Avian Pathol* 2012;41:239–250.
2. Cavanagh D, Naqi S. *Infectious Bronchitis in Diseases of Poultry*. Ames, Iowa: Iowa State University Press; 2003, pp. 101–119.
3. Cavanagh D. Severe acute respiratory syndrome vaccine development: experiences of vaccination against avian infectious bronchitis coronavirus. *Avian Pathol* 2003;32:567–582.
4. Cook JK. Protection of chickens against renal damage caused by a nephropathogenic infectious bronchitis virus. *Avian Pathol* 2001;30:423–426.
5. Shang J, Zheng Y, Yang Y, Liu C, Geng Q, *et al*. Cryo-em structure of infectious bronchitis coronavirus spike protein reveals structural and functional evolution of coronavirus spike proteins. *PLoS Pathog* 2018;14:e1007009.
6. Bickerton E. The S2 subunit of infectious bronchitis virus *Beaudette* is a determinant of cellular tropism. *J Virol* 2018;92.
7. Casais R, Dove B, Cavanagh D, Britton P. Recombinant avian infectious bronchitis virus expressing a heterologous spike gene demonstrates that the spike protein is a determinant of cell tropism. *J Virol* 2003;77:9084–9089.
8. Hodgson T. Recombinant infectious bronchitis coronavirus Beaudette with the spike protein gene of the pathogenic M41 strain remains attenuated but induces protective immunity. *J Virol* 2004;78:13804–13811.
9. Armesto M, Evans S, Cavanagh D, Abu-Median A-B, Keep S, *et al*. A recombinant avian infectious bronchitis virus expressing a heterologous spike gene belonging to the 4/91 serotype. *PLoS One* 2011;6:e24352.
10. Walls AC, Tortorici MA, Bosch B-J, Frenz B, Rottier PJM, *et al*. Cryo-electron microscopy structure of a coronavirus spike glycoprotein trimer. *Nature* 2016;531:114–117.
11. Yuan Y. Cryo-EM structures of MERS-CoV and SARS-CoV spike glycoproteins reveal the dynamic receptor binding domains. *Nat Commun* 2017;8:15092.
12. Gui M. Cryo-electron microscopy structures of the SARS-CoV spike glycoprotein reveal a prerequisite conformational state for receptor binding. *Cell Res* 2017;27:119–129.
13. Walls AC, Tortorici MA, Frenz B, Snijder J, Li W, *et al*. Glycan shield and epitope masking of a coronavirus spike protein observed by cryo-electron microscopy. *Nat Struct Mol Biol* 2016;23:899–905.
14. Ferris SP, Kodali VK, Kaufman RJ. Glycoprotein folding and quality-control mechanisms in protein-folding diseases. *Dis Model Mech* 2014;7:331–341.
15. Aebi M. N-linked protein glycosylation in the ER. *Biochima Biophysica Acta* 2013;1833:2430–2437.
16. Depetris RS. Partial enzymatic deglycosylation preserves the structure of cleaved recombinant HIV-1 envelope glycoprotein trimers. *J Biol Chem* 2012;287:24239–24254.
17. de Vries RP. The influenza A virus hemagglutinin glycosylation state affects receptor-binding specificity. *Virology* 2010;403:17–25.
18. Zheng J. Identification of N-linked glycosylation sites in the spike protein and their functional impact on the replication and infectivity of coronavirus infectious bronchitis virus in cell culture. *Virology* 2018;513:65–74.
19. Parsons L, Bouwman KM, Azurmendi H, de Vries RP, Cipollo JF, *et al*. Glycosylation of the viral attachment protein of Avian coronavirus is essential for host cell and receptor binding. *J Biol Chem* 2019;294:7797–7809.
20. Ben-Dor S. Biases and complex patterns in the residues flanking protein N-linked glycosylation sites. *Glycobiology* 2004;14:95–101.
21. Walls AC, Park Y-J, Tortorici MA, Wall A, McGuire AT, *et al*. Structure, function, and antigenicity of the SARS-CoV-2 spike glycoprotein. *Cell* 2020;181:281-292.
22. Watanabe Y. Site-specific glycan analysis of the SARS-CoV-2 spike. *Science* 2020;369:330–333.
23. Zhao P, Praissman JL, Grant OC, Cai Y, Xiao T, *et al*. Virus-receptor interactions of glycosylated SARS-CoV-2 spike and human ACE2 receptor. *Cell Host Microbe* 2020;28:586-601.
24. Abro SH. Bioinformatics and evolutionary insight on the spike glycoprotein gene of QX-like and *Massachusetts* strains of infectious bronchitis virus. *Virol J* 2012;9:211.
25. Mast SW, Moremen KW. *Family 47 α-Mannosidases in N-Glycan Processing, in Glycobiology*. 2006, pp. 31–46.
26. Schwarz F, Aebi M. Mechanisms and principles of N-linked protein glycosylation. *Curr Opin Struct Biol* 2011;21:576–582.
27. An Y. Comparative glycomics analysis of influenza Hemagglutinin (H5N1) produced in vaccine relevant cell platforms. *J Proteome Res* 2013;12:3707–3720.
28. Crispin M, Doores KJ. Targeting host-derived glycans on enveloped viruses for antibody-based vaccine design. *Curr Opin Virol* 2015;11:63–69.
29. Watanabe Y. Exploitation of glycosylation in enveloped virus pathobiology. *Biochim Biophys Acta Gen Subj* 2019;1863:1480–1497.
30. Walker LM. Broad and potent neutralizing antibodies from an African donor reveal a new HIV-1 vaccine target. *Science* 2009;326:285–289.
31. Lavine CL, Lao S, Montefiori DC, Haynes BF, Sodroski JG, *et al*. High-mannose glycan-dependent epitopes are frequently targeted in broad neutralizing antibody responses during human immunodeficiency virus type 1 infection. *J Virol* 2011;86:2153–2164.
32. Doores KJ. The HIV glycan shield as a target for broadly neutralizing antibodies. *FEBS J* 2015;282:4679–4691.
33. Yin Y. Glycosylation at 11Asn on hemagglutinin of H5N1 influenza virus contributes to its biological characteristics. *Vet Res* 2017;48:81.
34. Zhao D, Liang L, Wang S, Nakao T, Li Y, *et al*. Glycosylation of the hemagglutinin protein of H5N1 influenza virus increases its virulence in mice by exacerbating the host immune response. *J Virol* 2017;91.
35. Lee CD. A cross-neutralizing antibody between HIV-1 and influenza virus. *PLoS Pathog* 2021;17:e1009407.
36. Han DP, Lohani M, Cho MW. Specific asparagine-linked glycosylation sites are critical for DC-SIGN- and L-SIGN-mediated severe acute respiratory syndrome coronavirus entry. *J Virol* 2007;81:12029–12039.
37. Bouwman KM, Parsons LM, Berends AJ, de Vries RP, Cipollo JF, *et al*. Three amino acid changes in avian coronavirus spike protein allow binding to kidney tissue. *J Virol* 2020;94.
38. Behrens AJ, Harvey DJ, Milne E, Cupo A, Kumar A, *et al*. Molecular architecture of the cleavage-dependent mannose patch on a soluble HIV-1 envelope glycoprotein trimer. *J Virol* 2017;91.
39. An Y, Parsons LM, Jankowska E, Melnyk D, Joshi M, *et al*. N-glycosylation of seasonal influenza vaccine hemagglutinins: Implication for potency testing and immune processing. *J Virol* 2019;93.
40. Darbyshire JH. Taxonomic studies on strains of avian infectious bronchitis virus using neutralisation tests in tracheal organ cultures. *Arch Virol* 1979;61:227–238.
41. Britton P. Generation of a recombinant avian coronavirus infectious bronchitis virus using transient dominant selection. *J Virol Methods* 2005;123:203–211.

42. Cook JKA, Darbyshire JH, Peters RW. The use of chicken tracheal organ cultures for the isolation and assay of avian infectious bronchitis virus. *Arch Virol* 1976;50:109–118.
43. Van Roekel H, Clarke MK, Bullis KL, Olesiuk OM, Sperling FG. Infectious bronchitis. *Am J Vet Res* 1951;12:140–146.
44. Stevenson-Leggett P, Keep S, Bickerton E. Treatment with exogenous trypsin expands *in vitro* cellular tropism of the avian coronavirus infectious bronchitis virus. *Viruses* 2020;12:1102.
45. Hennion RM, Hill G. The preparation of chicken kidney cell cultures for virus propagation. *Methods Mol Biol* 2015;1282:57–62.
46. Dowgier G, Maier HJ. Quantification of coronaviruses by titration *In vitro* and *Ex vivo*. Maier H and Bickerton E (eds). In: *Coronaviruses: Methods and Protocols*. Springer Nature; 2020. pp. 135–143.
47. Mockett A, Cavanagh D, Brown DK. Monoclonal antibodies to the S1 spike and membrane proteins of avian infectious bronchitis Coronavirus strain Massachusetts M41. *Journal of General Virology* 1984;65:2281–2286.
48. Ellis S, Keep S, Britton P, de Wit S, Bickerton E, *et al*. Recombinant infectious bronchitis viruses expressing chimeric spike glycoproteins induce partial protective immunity against homologous challenge despite limited replication *in vivo*. *J Virol* 2018;92:23.
49. Reed LJ, Muench H. A simple method of estimating fifty per cent endpoints. *Am J Hyg* 1938;27.
50. Zhang C, Ye Z, Xue P, Shu Q, Zhou Y, *et al*. Evaluation of different N-glycopeptide enrichment methods for N-glycosylation sites mapping in mouse brain. *J Proteome Res* 2016;15:2960–2968.
51. Bern M, Kil YJ, Becker C. BYONIC: Advanced peptide and protein identification software. *Curr Protoc Bioinformatics* 2012;Chapter 13:Unit13.
52. Norris GE. The three-dimensional structure of PNGase F, a glycosylasparaginase from *Flavobacterium meningosepticum*. *Structure* 1994;2:1049–1059.
53. Tarentino AL, T.H.P. J, Maley F. The Release of Intact Oligosaccharides from specific Glycoproteins by Endo-B-N-acetylglucosaminidase H. *Journal of Biological Chemistry* 1974;249:818–824.
54. Valastro V. S1 gene-based phylogeny of infectious bronchitis virus: An attempt to harmonize virus classification. *Infect Genet Evol* 2016;39:349–364.
55. de Wit JJ, Cook JK, van der Heijden HM. Infectious bronchitis virus variants: a review of the history, current situation and control measures. *Avian Pathol* 2011;40:223–235.
56. Adzhar A. Molecular analysis of the 793/B serotype of infectious bronchitis virus in Great Britain. *Avian Pathol* 1997;26:625–640.
57. Cavanagh D. Location of the amino acid differences in the S1 spike glycoprotein subunit of closely related serotypes of infectious bronchitis virus. *Avian Pathol* 1992;21:33–43.
58. Bande F. Progress and challenges toward the development of vaccines against avian infectious bronchitis. *J Immunol Res, 2015* 2015:424860.
59. Keep S, Stevenson-Leggett P, Steyn A, Oade MS, Webb I, *et al*. Temperature sensitivity: A potential method for the generation of vaccines against the avian coronavirus infectious bronchitis virus. *Viruses* 2020;12.
60. Promkuntod N. Mapping of the receptor-binding domain and amino acids critical for attachment in the spike protein of avian coronavirus infectious bronchitis virus. *Virology* 2014;448:26–32.
61. Elbein AD, Tropea JE, Mitchell M, Kaushal GP. Kifunensine, a potent inhibitor of the glycoprotein processing mannosidase I. *J Biol Chem* 1990;265:15599–15605.
62. Kusters JG, Jager EJ, Lenstra JA, Koch G, Posthumus WP, *et al*. Analysis of an immunodominant region of infectious bronchitis virus. *J Immunol* 1989;143:2692–2698.
63. Maier HJ, Hawes PC, Cottam EM, Mantell J, Verkade P, *et al*. Infectious bronchitis virus generates spherules from zippered endoplasmic reticulum membranes. *mBio* 2013;4:e00801.
64. Corse E, Machamer CE. Infectious bronchitis virus E protein is targeted to the Golgi complex and directs release of virus-like particles. *J Virol* 2000;74:4319–4326.
65. Robinson M. Viral journeys on the intracellular highways. *Cell Mol Life Sci* 2018;75:3693–3714.
66. Delmas B, Laude H. Carbohydrate-induced conformational changes strongly modulate the antigenicity of coronavirus TGEV glycoproteins S and M. *Virus Res* 1991;20:107–120.
67. Gavrilov BK. Effects of glycosylation on antigenicity and immunogenicity of classical swine fever virus envelope proteins. *Virology* 2011;420:135–145.
68. Sun X. N-linked glycosylation of the hemagglutinin protein influences virulence and antigenicity of the 1918 pandemic and seasonal H1N1 influenza A viruses. *J Virol* 2013;87:8756–8766.
69. Wrapp D. Cryo-EM structure of the 2019-nCoV spike in the prefusion conformation. *Science* 2020;367:1260–1263.
70. Grant OC. Analysis of the SARS-CoV-2 spike protein glycan shield reveals implications for immune recognition. *Sci Rep* 2020;10:14991.
71. Wang S, Voronin Y, Zhao P, Ishihara M, Mehta N, *et al*. Glycan profiles of gp120 protein vaccines from four major HIV-1 subtypes produced from different host cell lines under Non-GMP or GMP conditions. *J Virol* 2020;94.
72. Li Z. The human coronavirus HCOV-229E s-protein structure and receptor binding. *Elife* 2019:8.
73. Yang TJ. Cryo-EM analysis of a feline coronavirus spike protein reveals a unique structure and camouflaging glycans. *Proc Natl Acad Sci U S A* 2020;117:1438–1446.
74. Raska M. Glycosylation patterns of HIV-1 gp120 depend on the type of expressing cells and affect antibody recognition. *J Biol Chem* 2010;285:20860–20869.
75. Pritchard LK, Spencer DIR, Royle L, Vasiljevic S, Krumm SA, *et al*. Glycan microheterogeneity at the PGT135 antibody recognition site on HIV-1 gp120 reveals a molecular mechanism for neutralization resistance. *J Virol* 2015;89:6952–6959.
76. Hargett AA, Wei Q, Knoppova B, Hall S, Huang Z-Q, *et al*. Defining HIV-1 envelope N-glycan microdomains through site-specific heterogeneity profiles. *J Virol* 2019;93.
77. Bonomelli C. The glycan shield of HIV is predominantly oligomannose independently of production system or viral clade. *PLoS One* 2011;6:e23521.
78. Butler M. Optimisation of the cellular metabolism of glycosylation for recombinant proteins produced by Mammalian cell systems. *Cytotechnology* 2006;50:57–76.
79. Ping J. Single-amino-acid mutation in the HA alters the recognition of H9N2 influenza virus by a monoclonal antibody. *Biochem Biophys Res Commun* 2008;371:168–171.
80. Doores KJ, Burton DR. Variable loop glycan dependency of the broad and potent HIV-1-neutralizing antibodies PG9 and PG16. *J Virol* 2010;84:10510–10521.
81. Zost SJ. Contemporary H3N2 influenza viruses have a glycosylation site that alters binding of antibodies elicited by egg-adapted vaccine strains. *Proc Natl Acad Sci U S A* 2017;114:12578–12583.
82. Doran RC. Characterization of a monoclonal antibody to a novel glycan-dependent epitope in the V1/V2 domain of the HIV-1 envelope protein, gp120. *Mol Immunol* 2014;62:219–226.
83. Andoh K. Decreased neutralizing antigenicity in IBV S1 protein expressed from mammalian cells. *Virus Res* 2015;208:164–170.
84. Wang L. Structural analysis of a highly glycosylated and unliganded gp120-based antigen using mass spectrometry. *Biochemistry* 2010;49:9032–9045.